PCCP

ROYAL SOCIETY OF CHEMISTRY

PAPER

View Article Online
View Journal | View Issue

Cite this: *Phys. Chem. Chem. Phys.*, 2023, **25**, 17403

Excitation wavelength dependent S_1-state decay dynamics of 2-aminopyridine and 3-aminopyridine†

Baihui Feng,[abc] Dongyuan Yang, *[a] Yanjun Min,[ac] Qinghua Gao,[ad] Benjie Fang,[b] Guorong Wu *[a] and Xueming Yang [ade]

Received 1st April 2023,
Accepted 5th June 2023

DOI: 10.1039/d3cp01487h

rsc.li/pccp

The decay dynamics of 2-aminopyridine and 3-aminopyridine excited to the S_1 state is investigated using femtosecond time-resolved photoelectron imaging. The lifetime of the S_1 state for both molecules shows a rapid decrease with the increase of the vibrational energy. It is shown that, besides intersystem crossing to the lower-lying triplet state of T_1, the decay to the ground state (S_0) *via* internal conversion through a conical intersection plays an increasingly important role and becomes dominant for vibrational states well above the S_1 state origin. The comparison between 2-aminopyridine and 3-aminopyridine suggests that the intramolecular hydrogen bonding between a hydrogen atom of the NH_2 group and the heterocyclic nitrogen atom in 2-aminopyridine effectively hinders the ring deformation at lower vibrational states which is required for the wavepacket to reach the S_1/S_0 conical intersection, and therefore slows down the S_1 to S_0 internal conversion.

I. Introduction

The photochemistry of small aromatic heterocyclic molecules offers an ideal prototype for understanding complicated photo-induced processes of large biologically relevant systems. For example, the photo-protective mechanism of biomolecules exposed to ultraviolet (UV) radiation has been better understood from the studies of lower excited-state decay dynamics of small heteroaromatic molecules, such as aromatic amino acids and nucleobases.[1–6] Ring structures containing heteroatoms of nitrogen (N) are quite common in nature and their photophysical and photochemical properties are of particular interest to both theorists and experimentalists. Pyrrole and pyridine are typical five-membered and six-membered heteroaromatic molecules, respectively. The photochemical behaviors of these isolated molecules, including a series of their derivatives, have been the subject of extensive studies for several decades.[7–19] In the last few years, we have investigated the ultrafast excited-state dynamics of pyrrole[20] and several of its methyl (or ethyl) substituted derivatives,[21–25] highlighting that the substitution effects are sensitive to the different substitution positions. Recently, we have also investigated the ultrafast decay dynamics of one of the substituted pyridines, 2-hydroxypyridine, excited to the S_1 electronic state in the pump wavelength range of 276.9–250.0 nm.[26] In this study, we continue our efforts on this topic and focus on two isomeric amines of pyridine, namely, 2-aminopyridine and 3-aminopyridine (hereafter termed simply 2-AP and 3-AP, respectively), with special interest in exploring the substitution position effects on the S_1 state decay dynamics. The chemical structures of 2-AP and 3-AP are presented schematically in Fig. 1.

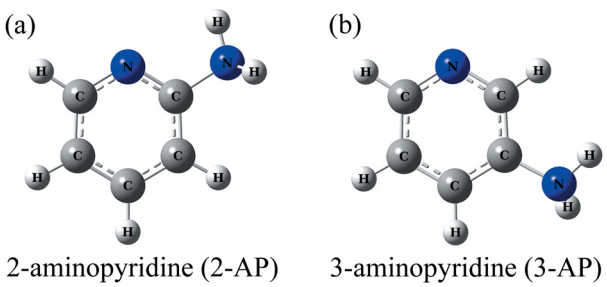

Fig. 1 Schematic representation of (a) 2-aminopyridine (2-AP) and (b) 3-aminopyridine (3-AP).

[a] *State Key Laboratory of Molecular Reaction Dynamics, Dalian Institute of Chemical Physics, Chinese Academy of Sciences, 457 Zhongshan Road, Dalian, Liaoning 116023, China. E-mail: yangdy@dicp.ac.cn, wugr@dicp.ac.cn*
[b] *Key Laboratory of Chemical Lasers, Dalian Institute of Chemical Physics, Chinese Academy of Sciences, 457 Zhongshan Road, Dalian, Liaoning 116023, China*
[c] *University of Chinese Academy of Sciences, Beijing 100049, China*
[d] *Hangzhou Institute of Advanced Studies, Zhejiang Normal University, 1108 Gengwen Road, Hangzhou, Zhejiang 311231, China*
[e] *Department of Chemistry, College of Science, Southern University of Science and Technology, Shenzhen 518055, China*

† Electronic supplementary information (ESI) available. See DOI: https://doi.org/10.1039/d3cp01487h

The first absorption band in the near-UV region of 2-AP and 3-AP corresponds to a $\pi^* \leftarrow \pi$ electronic transition. The 0–0 band origin of the $S_1 \leftarrow S_0$ electronic transition was found to be at 33471 cm^{-1} (298.8 nm) for 2-AP[27–33] and 33050 cm^{-1} (302.6 nm) for 3-AP.[29,34] In a high-resolution, rotationally resolved $S_1 \leftarrow S_0$ electronic spectrum of 2-AP at $\sim$299 nm, a lifetime of $\sim$1.5 ns was estimated from the Lorentzian linewidth of individual rotational lines.[35] This time constant of 1.5 ns is consistent with the measured fluorescence lifetime of $\leq$2 ns for the bare 2-AP molecule in the gas phase[30,36] and the estimated value for the S_1 origin level in a time-delayed two-color photoelectron spectral study using picosecond laser pulses with 100 ps time intervals.[37] Later on, in two femtosecond time-resolved pump–probe mass spectroscopy studies, lifetimes of 1.5 ns and 11 ps were derived for the S_1 state origin and vibrational levels of 0.81 eV above the origin, respectively.[38,39] The direct time-resolved studies of the excited-state dynamics of 3-AP are scarce. It was reported that the lifetime of the S_1 state ($v = 0$) of 3-AP is about 0.4 ns.[37]

An intersystem crossing (ISC) process from the S_1 to the T_1 electronic state was revealed in the time-delayed two-color photoionization photoelectron spectral study.[37] The corresponding photoelectron signal which was assigned to ionization from the T_1 state to the ground state (D_0) of the 2-AP cation clearly shows a rise with a maximum delay of 5 ns employed. In addition, the involvement of the T_2 or the T_3 state was eliminated based on a combined consideration of the values of the electronic energies, the configuration interaction calculations (the electronic overlap between the molecular orbitals of the excited state neutrals and the ions) and the observed photoelectron spectra. In a previous theoretical study of 2-AP, Fang and coworkers carried out *ab initio* calculations to identify the contributions from the possible radiative and nonradiative channels of the S_1 state.[40] Their calculations showed an ultrashort nonradiative process (internal conversion (IC) to the ground state through the S_1/S_0 conical intersection (CI)) for the S_1 state of 2-AP, involving a ring deformation reaction pathway on the S_1 state potential energy surface (PES). They also pointed out that the calculated lifetime of the S_1 state is very sensitive to the barrier height along the reaction path of the ring deformation.

In this paper, we present a femtosecond time-resolved photoelectron imaging (fs-TRPEI) study of the $S_1(^1\pi\pi^*)$ state decay dynamics of 2-AP and 3-AP in a broad pump wavelength range. The clear pump wavelength dependence of the decay dynamics is analyzed in detail and the substitution position effects on the S_1 state decay dynamics are also discussed. This study provides a comprehensive picture of the S_1 state decay dynamics of 2-AP and 3-AP.

II. Experimental

The fs-TRPEI experiment was carried out on a velocity map imaging (VMI) spectrometer[41] and the detailed experimental methods have been described in our earlier publications.[22,42] So only a brief description of the key features will be given here. Both the 2-AP and 3-AP samples were a white crystalline solid purchased commercially from Macklin (98% purity for 2-AP and 99% purity for 3-AP) and used directly without further purification. The sample was heated to 50 °C, mixed with about 2 bar of helium carrier gas and expanded supersonically into a high vacuum source chamber *via* a pulsed Even-Lavie valve operating at 1 kHz. The seeded molecular beam entered the interaction chamber of the VMI spectrometer through a 1 mm skimmer (Beam Dynamics Inc., Model 1) located 40 mm downstream from the nozzle orifice.

The laser system consisted of a fully integrated Ti:sapphire oscillator–regenerative amplifier (Coherent, Libra-HE) and two commercial optical parametric amplifiers (OPA, Coherent, OPerA Solo), each pumped by a fraction (1.3 mJ per pulse) of the fundamental 800 nm output of the 1 kHz amplifier. The pump laser pulse in the wavelength range of 260.0–302.5 nm (0.2–1.2 μJ per pulse) was produced from one of the OPAs. The bandwidth of the pump laser was 290–440 cm^{-1} at full width at half maximum (FWHM). The probe laser pulse was chosen at 239.3 nm (0.1–0.8 μJ per pulse, $\sim$170 cm^{-1} bandwidth) and obtained by doubling the output of the other OPA at 478.6 nm using a 0.15 mm β-barium borate (BBO) crystal. The pump–probe time delay was precisely controlled using a linear translation stage (Newport, M-ILS250HA) located at the upstream of the second OPA. The two laser pulses were combined collinearly on a dichroic mirror without further compression and then focused using a calcium fluoride lens (f/75) into the interaction region of the VMI spectrometer to intersect the seeded molecular beam. Both the pump and probe pulses were linearly polarized and the polarization direction was parallel to the micro-channel plate (MCP)/phosphor screen detector. The laser pulse energy and beam-focusing condition were adjusted for an optimized signal-to-noise ratio.

The 2D photoelectron images at different pump–probe time delays were recorded using a computer-controlled camera and transferred to 3D distributions using the pBasex Abel inversion method.[43] The time-dependent photoelectron 3D distributions were integrated along the recoiling angle to derive the photoelectron kinetic energy distributions, *i.e.*, TRPES. The background photoelectron signal generated by one-color photoionization of the sample had been subtracted. Electron kinetic energy calibration was performed using multiphoton ionization of the Xe atoms.[41] The two-color non-resonant ionization of the NO molecules was utilized to measure the time-zero and cross-correlation (*i.e.*, instrumental response function (IRF)) between the pump and the probe laser pulse. The IRF was measured to be 155 $\pm$ 15 fs (FWHM) based on the approximation that both pump and probe laser pulses possessed a Gaussian profile.

The molecular beam has been carefully optimized to minimize the presence of 2-AP and 3-AP clusters since their clusters are easily generated in a supersonic molecular beam.[38,39,44–47] The heating temperature of the sample was kept at a relatively low temperature of 50 °C. We also modified the pulsed valve parameters, such as the opening time and time delay between the molecular beam and the laser pulse. The time-of-flight (TOF) mass spectrum was carefully checked before and after

TRPES measurements to verify that there was no observable cluster under our molecular beam condition.

III. Results and discussion

The analysis of TRPES

In Fig. 2(a), the TRPES spectrum of 2-AP at a pump wavelength of 298.2 nm is shown. It exhibits two broad features, a strong one centered at 1.0 eV and the other very weak one centered at 0.2 eV. In Fig. 2(b), photoelectron kinetic energy distributions at a few selected delays are presented, clearly showing the two distinct features. In Fig. 2(c), photoelectron transients for these two features (integrated over kinetic energy ranges of 0.01–0.30 eV and 0.60–1.20 eV, respectively) are shown. A very weak probe–pump signal, representing the signal from a process in which the probe photon excites 2-AP to an electronically excited state and the pump photon ionizes the excited 2-AP, also appears at lower photoelectron kinetic energies, as shown in the inset of Fig. 2(c). A simple fit with single exponential decay extracts a lifetime of 1.1 ns and $\gg$1 ns for the higher and lower kinetic energy features, respectively.

All TRPES spectra for 2-AP at pump wavelengths of 298.2, 293.1, 280.1, 270.1 and 260.1 nm are shown in Fig. 3(a–e). The dynamics becomes progressively shorter with the decrease of the pump wavelength. With the decrease of the pump wavelength, the probe–pump signal at negative delays becomes stronger and stronger, presumably due to a decreasing absorption cross-section of the pump laser pulse with the decrease of the pump wavelength. In order to derive more detailed information, a 2D global least-squares method is employed here to simultaneously fit the TRPES data (Fig. 3(a–e)) at all time delays and photoelectron kinetic energies. The model used here can be expressed using the following equation:

$$S(t,\varepsilon_k) = A_0(\varepsilon_k)\times \mathrm{IRF} + \sum_{i=1}^{n(\leq 3)} A_i(\varepsilon_k)\times\left\{\left[H(t)\times\exp\left(-\frac{t}{\tau_i}\right)\right]\otimes \mathrm{IRF}\right\} + A_4(\varepsilon_k)\times\left\{\left[H(-t)\times\exp\left(-\frac{-t}{\tau_4}\right)\right]\otimes \mathrm{IRF}\right\} \quad (1)$$

where $S(t,\varepsilon_k)$ represents the 2D TRPES spectrum, while t and ε_k are the pump–probe time delay and the kinetic energy of the emitted photoelectron, respectively. $A_i(\varepsilon_k) \times \exp(-t/\tau_i)$ is the contribution with lifetime τ_i and amplitude $A_i(\varepsilon_k)$. $H(t)$ is the Heaviside step function. The IRF is the 1 + 1′ cross-correlation between the pump and probe laser pulses, which is measured independently. $A_0(\varepsilon_k) \times$ IRF describes the contribution from the non-resonant two-color (1 + 1′) signal. It should be mentioned that an additional component ($A_4(\varepsilon_k)$) standing for the signal at negative time delays associated with the probe–pump dynamics is also included for a proper description of the TRPES data. An overall very satisfactory fit to the 2D TRPES spectra is achieved. The derived time constants and the photoelectron kinetic energy dependent amplitudes of each component are shown in Fig. 3(f–j). The probe–pump component is not shown here and will not be further discussed since it is out of the concern of this work.

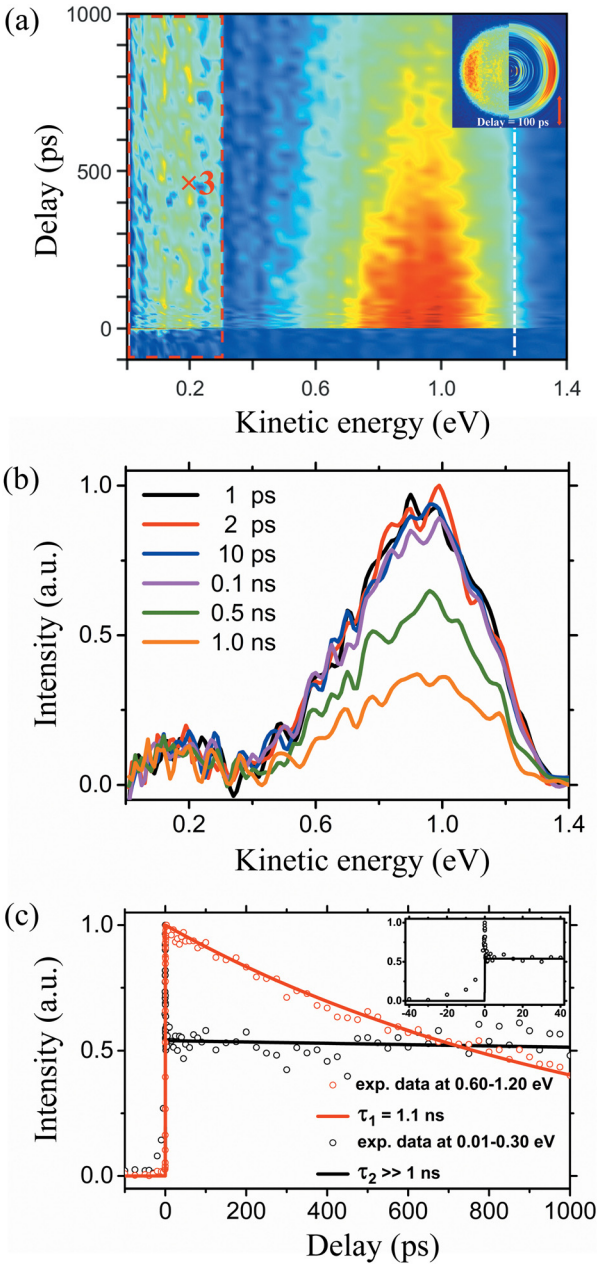

Fig. 2 (a) TRPES spectrum of 2-AP at a pump wavelength of 298.2 nm after subtracting the background photoelectrons generated from single-color multiphoton ionization. A portion of it (below 0.30 eV) is scaled up by a factor of 3 for a better presentation. The inset shows the background subtracted and 4-fold symmetrized photoelectron image at a 100 ps time delay, with the left and right halves representing the raw and deconvoluted images, respectively. The red double arrow indicates the polarization direction of the pump and probe lasers. (b) The photoelectron kinetic energy distributions at selected pump–probe time delays. (c) Normalized photoelectron transients (from −100 to 1000 ps) derived by summing up the TRPES spectrum in two different kinetic energy ranges, 0.01–0.30 eV and 0.60–1.20 eV. The symbols show the experimental data, while the lines show the fits to the experimental data. The inset shows the transient (0.01–0.30 eV) from −40 to 40 ps.

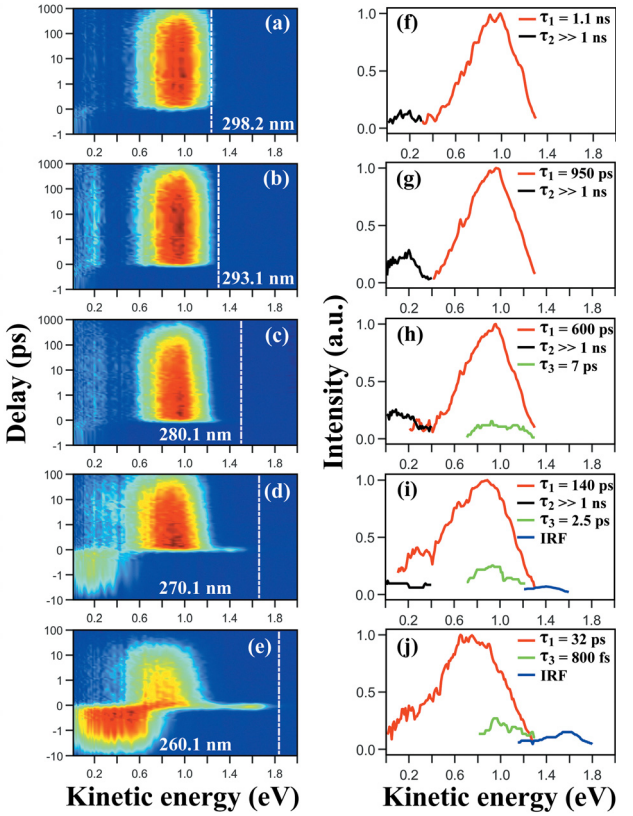

Fig. 3 (a–e) TRPES spectra of 2-AP at pump wavelengths of 298.2, 293.1, 280.1, 270.1 and 260.1 nm, respectively, after subtracting the background photoelectrons generated from single-color multiphoton ionization. Note that a combination of linear (between −1 and 1 ps) and logarithmic (≤ −1 or/and ≥ 1 ps) scales is used in the ordinate. The energy limits for two-color (1 + 1′) ionization to the ground state (D_0) of the 2-AP cation, calculated using an adiabatic ionization potential of 8.11 eV (ref. 32 and 33), are indicated by the white dash-dot lines. (f–j) The photoelectron kinetic energy dependent amplitudes of each component derived from a 2D global least-squares fit to the data.

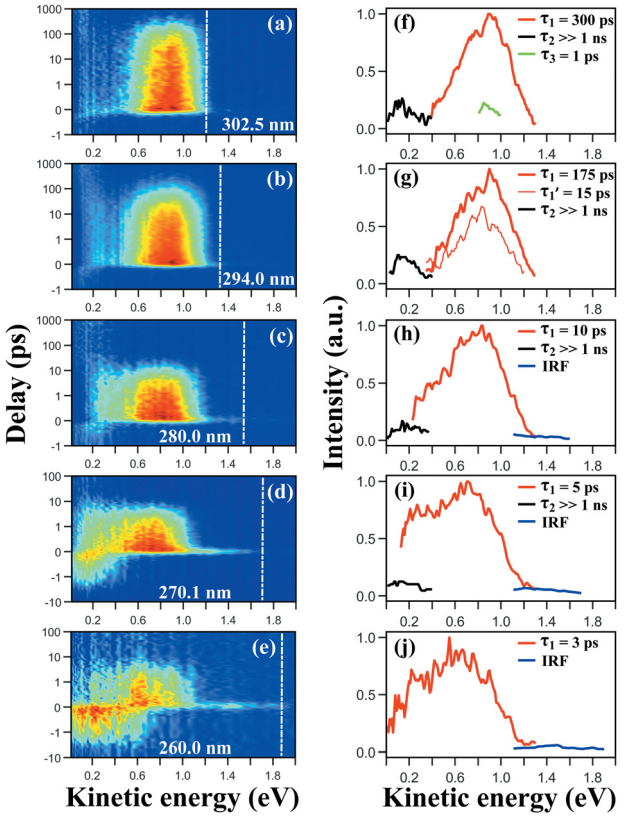

Fig. 4 (a–e) TRPES spectra of 3-AP at pump wavelengths of 302.5, 294.0, 280.0, 270.1 and 260.0 nm, respectively, after subtracting the background photoelectrons generated from single-color multiphoton ionization. Note that a combination of linear (between −1 and 1 ps) and logarithmic (≤−1 or/and ≥1 ps) scales is used in the ordinate. The energy limits for two-color (1 + 1′) ionization to the ground state (D_0) of the 3-AP cation, calculated using an adiabatic ionization potential of 8.09 eV (ref. 34), are indicated by the white dash-dot lines. (f–j) The photoelectron kinetic energy dependent amplitudes of each component derived from a 2D global least-squares fit to the data.

The TRPES spectra of 3-AP at pump wavelengths of 302.5, 294.0, 280.0, 270.1 and 260.0 nm are presented in Fig. 4(a–e). An analogous analysis was performed and the results are shown in Fig. 4(f–j).

The assignments of the time constants

Two time constants, 1.1 ± 0.1 ns and ≫ 1 ns, are derived for 2-AP at 298.2 nm, with the latter only being associated with photoelectrons of very lower kinetic energies. The pump wavelength of 298.2 nm corresponds to the S_1 origin and a few low energy vibrational levels covered by the intrinsic broad bandwidth (~400 cm^{-1}) of the pump laser pulse are expected to be excited. It is therefore straightforward to assign the time constant of 1.1 ± 0.1 ns to the lifetime of the $S_1(^1\pi\pi^*)$ origin level and several S_1 low energy vibrational levels. This derived lifetime is consistent with previous studies.[30,36,37] An ISC process from the S_1 to the T_1 electronic state was also revealed in a time-delayed two-color photoionization photoelectron spectral study.[37] Therefore, we assign the time constant of ≫ 1 ns (including pump wavelengths of 298.2, 293.1 and 280.1 nm) to the lifetime of the T_1 state. A comparison of photoelectron kinetic energy distributions between these previous measurements (using the 200 nm picosecond probe pulse)[37] and our work here (using the 239.3 nm femtosecond probe pulse) supports the above assignment, and the reason why there is no significant delayed rise for the signal at the lower kinetic energy centered at 0.2 eV is explained in terms of the overlap in the photoelectron signal between the S_1 and the T_1 state (detailed in the ESI†). In addition, the much lower excitation energy of the T_1 state[37,48] causes the photoelectrons associated with it appearing at much lower kinetic energies and rules out the direct excitation of the T_1 state here. At 270.1 and 260.1 nm, this component becomes too weak to be recognized.

With the decrease of the pump wavelength, the lifetime associated with the S_1 state (1.1 ± 0.1 ns at 298.2 nm) decreases rapidly, becomes 950 ± 100, 600 ± 100, 140 ± 40 and 32 ± 5 ps for 293.1, 280.1, 270.1 and 260.1 nm pump wavelengths, respectively.

At the three shortest pump wavelengths, 280.1, 270.1 and 260.1 nm, a much smaller time constant (7 ± 3 ps at 280.1 nm,

2.5 ± 0.5 ps at 270.1 nm and 800 ± 300 fs at 260.1 nm) is also involved, associated with a much weaker feature at higher kinetic energies. Considering the overall similarities of TRPES spectra at all the pump wavelengths and continuous change of the time constants, no second electronic state is expected to be accessed at the three shortest pump wavelengths. This is further supported by the analysis of the time-resolved photoelectron angular distributions (TRPADs) which shows virtually identical PADs for all pump wavelengths and constant PAD at all delays for each pump wavelength (see Fig. S1 in the ESI†). We assign these time constants to an intramolecular vibrational energy redistribution (IVR) process during the initial relaxation of the wavepacket out of the Franck–Condon (FC) region, accompanied by a distinct decrease of photoionization efficiency. Due to this change in photoionization efficiency, two different time constants are needed in the simulation of a continuous evolution of the wavepacket on a single PES. A weak two-color non-resonant photoelectron signal also appears at pump wavelengths of 270.1 and 260.1 nm, termed the IRF in Fig. 3(i and j).

The time constants derived from the analysis of the TRPES spectra of 3-AP can be assigned in a similar way. The major component of the TRPES spectrum at each pump wavelength (300 ± 50 ps at 302.5 nm, 175 ± 50 and 15 ± 5 ps at 294.0 nm, 10 ± 2 ps at 280.0 nm, 5 ± 1 ps at 270.1 nm and 3 ± 1 ps at 260.0 nm) is assigned to the depopulation of the S_1 state. For 294.0 nm, there are two time constants (labelled as τ_1 and τ_1' in Fig. 4(g)) which are assigned to be associated with the lifetime of the S_1 state. This is most likely due to the fact that the vibrational states composing the wavepacket possess distinct rates of decay out of the S_1 PES and therefore two time constants were needed in the fit of the TRPES spectrum, consistent with the experimental result that the lifetime of the S_1 state shows a strong dependence on the vibrational energy. The vibrational states corresponding to 175 ± 50 and 15 ± 5 ps might be of different modes and therefore show distinct effects in promoting the nonadiabatic decay of the S_1 state. However, we are unable to identify them for now due to the lack of the vibrationally resolved structure in the TRPES spectrum. A minor component of 1.0 ± 0.5 ps at 302.5 nm is assigned to the initial IVR process of the wavepacket, similar to those observed for 2-AP. This IVR process is not identified at the other pump wavelengths for 3-AP. The contribution from the T_1 state which is populated *via* ISC from the initially excited S_1 state seems to appear at 302.5, 294.0, 280.0, and 270.1 nm, but becomes weaker and weaker with the decrease of the pump wavelength and finally unrecognizable at 260.0 nm. Again, there is no indication in our TRPES data of 3-AP that an additional higher-lying electronic state (*i.e.*, the second bright $^1\pi\pi^*$ state) starts to be involved even at the shortest pump wavelength of 260.0 nm. The second $^1\pi\pi^*$ state is expected to be accessed at deeper UV wavelengths.

Decay dynamics of the S_1 state of 2-AP and 3-AP

Both 2-AP and 3-AP show a rapid decrease of the S_1 state lifetime with the decrease of the pump wavelength, *i.e.*, the increase of the vibrational energy. For low energy vibrational levels of the S_1 state, the ISC process to the lower-lying T_1 state is suggested to be one of the decay channels and identified in our TRPES spectra. With the increase of the vibrational energy, the lifetime of the S_1 state becomes increasingly smaller and the ISC channel becomes increasingly more minor, suggesting that the decay to the S_0 state through the S_1/S_0 CI becomes the dominant channel. At higher excitation energies, the channel of IC from the $S_1(^1\pi\pi^*)$ state to a lower-lying $^1n\pi^*$ state may be in operation. However, the conical intersection between the $^1\pi\pi^*$ and $^1n\pi^*$ states of 2-AP was calculated to be at an energy of 4.75 eV with almost planar geometry[39] and is therefore not accessible with the excitation wavelengths employed here, except the shortest pump wavelength (~260 nm, 4.77 eV). There is no evidence in our TRPES spectra that this channel plays a role in the decay dynamics of the S_1 state of both 2-AP and 3-AP.

Most interesting insights come from the comparison between 2-AP and 3-AP. In Fig. 5, the vibrational energy dependence of the S_1 state lifetime is compared. 3-AP shows a much more rapid decay rate than 2-AP, especially at lower vibrational energies. We rationalize this in terms of the difference in the barrier height along the ring deformation coordinate on the S_1 state PES. In a combination of absorption and single vibronic level (SVL) fluorescence spectral study of 2-AP,[28,49] it was evidenced that the NH_2 inversion in 2-AP is affected by the intramolecular hydrogen bonding between the ring nitrogen atom and the one hydrogen atom of the NH_2 group. This intramolecular hydrogen bonding also draws one of the hydrogen atoms of the NH_2 group closer to the ring nitrogen atom and results in a more planar geometry. For 3-AP, this effect does not exist because the hydrogen atoms of the NH_2 group in the 3-position are too distant from the in-ring nitrogen atom to form such intramolecular hydrogen bonding. Therefore, for 3-AP, ring deformation occurs more easily and facilitates the initially excited wavepacket to evolve to the S_1/S_0 CI and funnel into the S_0 state.

We summarize the experimental findings as follows: the S_1 state of both 2-AP and 3-AP has two nonradiative decay

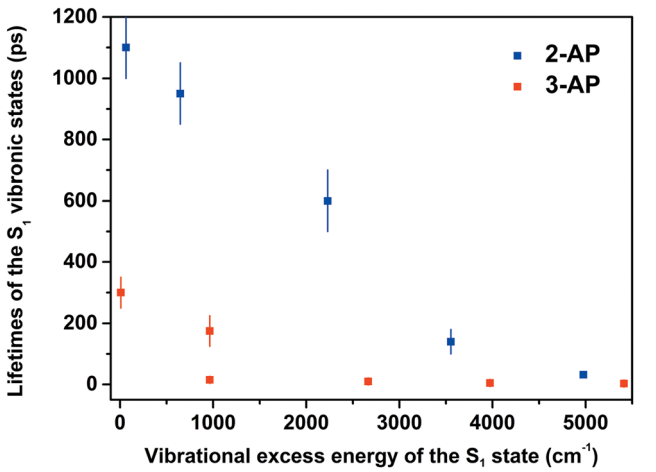

Fig. 5 Comparison of the vibrational energy dependence of the S_1 state lifetime.

channels: ISC to the T_1 triplet state and IC to the ground state *via* the S_1/S_0 CI, with the latter dominating at higher vibrational levels. The intramolecular hydrogen bonding between a hydrogen atom of the NH_2 group and the heterocyclic nitrogen atom in 2-AP significantly increases the barrier height along the ring deformation coordinates, resulting in a much slower deactivation rate, especially at lower vibrational energies.

IV. Conclusions

In conclusion, we investigate the S_1 state decay dynamics of 2-AP and 3-AP excited around the S_1 origin and also at higher excitation energies using the fs-TRPEI technique. Both molecules show a rapid decrease of the S_1 state lifetime with the increase of the vibrational energy. At lower vibrational energies, the nonradiative decay channel of ISC to the lower-lying T_1 triplet state is in operation. At higher excitation energies, IC to the S_0 state becomes dominant. 2-AP shows a much slower decay rate of the S_1 state, especially at lower vibrational energies. This is due to an intramolecular hydrogen bonding between a hydrogen atom of the NH_2 group and the heterocyclic nitrogen atom in 2-AP which hinders the ring deformation and increases the barrier height between the FC region and the S_1/S_0 CI. This fs-TRPEI study over a broad pump wavelength range for both 2-AP and 3-AP provides very detailed information on the S_1 state decay dynamics, highlighting how the different substitution positions may affect the decay dynamics of electronically excited heteroaromatic molecules differently.

Author contributions

Xueming Yang and Guorong Wu conceived the experiments. Baihui Feng and Dongyuan Yang carried out the experiments, analysed the data and prepared the manuscript. Yanjun Min, Qinghua Gao and Benjie Fang contributed to the data discussion and interpretation. Dongyuan Yang and Guorong Wu edited, discussed and approved the whole paper.

Conflicts of interest

There are no conflicts to declare.

Acknowledgements

This work was financially supported by the National Natural Science Foundation of China (No. 21833003, 22203095, and 22288201), the Key Technology Team of the Chinese Academy of Sciences (GJJSTD20220001) and the Strategic Priority Research Program of the Chinese Academy of Sciences (No. XDB17000000). The authors also gratefully acknowledge the support from the Dalian Coherent Light Source (DCLS).

References

1 S. Ullrich, T. Schultz, M. Z. Zgierski and A. Stolow, *Phys. Chem. Chem. Phys.*, 2004, **6**, 2796–2801.
2 C. E. Crespo-Hernández, B. Cohen, P. M. Hare and B. Kohler, *Chem. Rev.*, 2004, **104**, 1977–2019.
3 C. Canuel, M. Mons, F. Piuzzi, B. Tardivel, I. Dimicoli and M. Elhanine, *J. Chem. Phys.*, 2005, **122**, 074316.
4 G. M. Roberts and V. G. Stavros, *Chem. Sci.*, 2014, **5**, 1698–1722.
5 B. Marchetti, T. N. V. Karsili, M. N. R. Ashfold and W. Domcke, *Phys. Chem. Chem. Phys.*, 2016, **18**, 20007–20027.
6 S. Boldissar and M. S. de Vries, *Phys. Chem. Chem. Phys.*, 2018, **20**, 9701–9716.
7 D. A. Blank, S. W. North and Y. T. Lee, *Chem. Phys.*, 1994, **187**, 35–47.
8 J. Wan, J. Meller, M. Hada, M. Ehara and H. Nakatsuji, *J. Chem. Phys.*, 2000, **113**, 7853–7866.
9 B. O. Roos, P.-Å. Malmqvist, V. Molina, L. Serrano-Andrés and M. Merchán, *J. Chem. Phys.*, 2002, **116**, 7526–7536.
10 J. Wei, J. Riedel, A. Kuczmann, F. Renth and F. Temps, *Faraday Discuss.*, 2004, **127**, 267–282.
11 B. Cronin, M. G. D. Nix, R. H. Qadiri and M. N. R. Ashfold, *Phys. Chem. Chem. Phys.*, 2004, **6**, 5031–5041.
12 H. Lippert, H. H. Ritze, I. V. Hertel and W. Radloff, *ChemPhysChem*, 2004, **5**, 1423–1427.
13 M. Staniforth, J. D. Young, D. R. Cole, T. N. V. Karsili, M. N. R. Ashfold and V. G. Stavros, *J. Phys. Chem. A*, 2014, **118**, 10909–10918.
14 V. Ovejas, R. Montero, M. Fernández-Fernández and A. Longarte, *J. Phys. Chem. A*, 2015, **119**, 3355–3365.
15 L. Blancafort, V. Ovejas, R. Montero, M. Fernández-Fernández and A. Longarte, *J. Phys. Chem. Lett.*, 2016, **7**, 1231–1237.
16 M. Chachisvilis and A. H. Zewail, *J. Phys. Chem. A*, 1999, **103**, 7408–7418.
17 Z.-L. Cai and J. R. Reimers, *J. Phys. Chem. A*, 2000, **104**, 8389–8408.
18 H. Wang, C. Zhu, J.-G. Yu and S. H. Lin, *J. Phys. Chem. A*, 2009, **113**, 14407–14414.
19 P. C. Varras, P. S. Gritzapis and K. C. Fylaktakidou, *Mol. Phys.*, 2018, **116**, 154–170.
20 G. Wu, S. P. Neville, O. Schalk, T. Sekikawa, M. N. R. Ashfold, G. A. Worth and A. Stolow, *J. Chem. Phys.*, 2015, **142**, 074302.
21 G. Wu, S. P. Neville, O. Schalk, T. Sekikawa, M. N. R. Ashfold, G. A. Worth and A. Stolow, *J. Chem. Phys.*, 2016, **144**, 014309.
22 D. Yang, Z. Chen, Z. He, H. Wang, Y. Min, K. Yuan, D. Dai, G. Wu and X. Yang, *Phys. Chem. Chem. Phys.*, 2017, **19**, 29146–29152.
23 D. Yang, Y. Min, Z. Chen, Z. He, K. Yuan, D. Dai, X. Yang and G. Wu, *Phys. Chem. Chem. Phys.*, 2018, **20**, 15015–15021.
24 W. Yuan, D. Yang, B. Feng, Y. Min, Z. Chen, S. Yu, G. Wu and X. Yang, *Phys. Chem. Chem. Phys.*, 2021, **23**, 17625–17633.
25 W. Yuan, B. Feng, D. Yang, Y. Min, S. Yu, G. Wu and X. Yang, *Chin. J. Chem. Phys.*, 2021, **34**, 386–392.

26 Y. Min, W. Yuan, D. Yang, D. Dai, S. Yu, G. Wu and X. Yang, *Chin. J. Chem. Phys.*, 2022, **35**, 242–248.
27 J. M. Hollas, G. H. Kirby and R. A. Wright, *Mol. Phys.*, 1970, **18**, 327–335.
28 J. M. Hollas, H. Musa and T. Ridley, *J. Mol. Spectrosc.*, 1984, **104**, 89–106.
29 R. D. Gordon, D. Clark, J. Crawley and R. Mitchell, *Spectrochim. Acta, Part A*, 1984, **40**, 657–668.
30 J. Hager and S. C. Wallace, *J. Phys. Chem.*, 1985, **89**, 3833–3841.
31 B. Kim, N. Thantu and P. M. Weber, *J. Chem. Phys.*, 1992, **97**, 5384–5391.
32 S. J. Baek, K.-W. Choi, Y. S. Choi and S. K. Kim, *J. Chem. Phys.*, 2002, **117**, 2131–2140.
33 J. L. Lin, R. H. Wu and W. B. Tzeng, *Chem. Phys. Lett.*, 2002, **353**, 55–62.
34 J. L. Lin, R. H. Wu and W. B. Tzeng, *Chem. Phys.*, 2002, **280**, 191–203.
35 D. R. Borst, J. R. Roscioli and D. W. Pratt, *J. Phys. Chem. A*, 2002, **106**, 4022–4027.
36 J. W. Hager, G. W. Leach, D. R. Demmer and S. C. Wallace, *J. Phys. Chem.*, 1987, **91**, 3750–3758.
37 B. Kim, C. P. Schick and P. M. Weber, *J. Chem. Phys.*, 1995, **103**, 6903–6913.
38 E. Samoylova, V. R. Smith, H.-H. Ritze, W. Radloff, M. Kabelac and T. Schultz, *J. Am. Chem. Soc.*, 2006, **128**, 15652–15656.
39 E. Samoylova, W. Radloff, H.-H. Ritze and T. Schultz, *J. Phys. Chem. A*, 2009, **113**, 8195–8201.
40 F. Zhang, Y. Ai, Y. Luo and W. Fang, *J. Chem. Phys.*, 2009, **130**, 144315.
41 Z. He, Z. Chen, D. Yang, D. Dai, G. Wu and X. Yang, *Chin. J. Chem. Phys.*, 2017, **30**, 247–252.
42 D. Yang, Y. Min, B. Feng, X. Yang and G. Wu, *Phys. Chem. Chem. Phys.*, 2022, **24**, 22710–22715.
43 G. A. Garcia, L. Nahon and I. Powis, *Rev. Sci. Instrum.*, 2004, **75**, 4989–4996.
44 T. Schultz, E. Samoylova, W. Radloff, I. V. Hertel, A. L. Sobolewski and W. Domcke, *Science*, 2004, **306**, 1765–1768.
45 R. Wu and B. Brutschy, *J. Phys. Chem. A*, 2004, **108**, 9715–9720.
46 Y. Yamada, N. Mikami and T. Ebata, *Proc. Natl. Acad. Sci. U. S. A.*, 2008, **105**, 12690–12695.
47 P. Ottiger, J. A. Frey, H.-M. Frey and S. Leutwyler, *J. Phys. Chem. A*, 2009, **113**, 5280–5288.
48 S. Hotchandani and A. C. Testa, *J. Chem. Phys.*, 1973, **59**, 596–600.
49 J. M. Hollas, H. Musa and T. Ridley, *J. Mol. Spectrosc.*, 1984, **104**, 107–121.